Lewis acid-catalyzed Diels–Alder cycloaddition of 2,5-dimethylfuran and ethylene

Chellegui, Mohamed; Champagne, Benoît; Trabelsi, Mahmoud

Published in:
Theoretical Chemistry Accounts

DOI:
10.1007/s00214-022-02880-y

Publication date:
2022

Document Version
Publisher's PDF, also known as Version of record

Theoretical Chemistry Accounts (2022) 141:21
https://doi.org/10.1007/s00214-022-02880-y

REGULAR ARTICLE

Lewis acid-catalyzed Diels–Alder cycloaddition of 2,5-dimethylfuran and ethylene: a density functional theory investigation

Mohamed Chellegui[1,2] · Benoît Champagne[2] · Mahmoud Trabelsi[1]

Received: 24 April 2021 / Accepted: 8 March 2022

Abstract
Density functional theory calculations with the M06-2X exchange–correlation functional have been performed to explore the Diels–Alder reaction between 2,5-DMF and ethylene as well as to compare the uncatalyzed reaction to the one catalyzed by the $AlCl_3$ Lewis acid. The uncatalyzed reaction corresponds to a normal electron-demand (NED) mechanism where ethylene is an electron acceptor and 2,5-DMF plays the role of electron donor. This reaction presents a low polar character, its kinetics is little impacted by the solvent dielectric constant, and the formation of the two new σ bonds occurs through a one-step synchronous process. When the LA interacts with ethylene, forming a π-complex, it enhances its acceptor character, further favoring the NED mechanism, which is accompanied by a reduction of the free energy of the transition state. On the other hand, when $AlCl_3$ is complexed by 2,5-DMF, the inverse electron-demand (IED) mechanism is favored, with ethylene playing the role of the donor. Within both NED and IED mechanism, the LA-catalyzed reaction takes place via a one-step asynchronous process. In addition, it is highly polar, so that the activation barrier decreases with the solvent polarity. Moreover, the calculations have evidenced that the LA forms stable complexes with any of the reactants so that the gain on the activation barrier amounts to 9–12 kcal mol^{-1} for the NED mechanism and to 3–9 kcal mol^{-1} for the IED one and that the formation of Al_2Cl_6 dimers impacts the different equilibria. Finally, the decrease of the activation barrier goes in pair with the reduction of the HOMO–LUMO gap, with the greatest decrease recorded when the LA interacts with ethylene according to the NED mechanism.

Keywords Diels–Alder reaction · 2,5-DMF and ethylene · Lewis acid catalysis · DFT calculations

1 Introduction

Nowadays, fossil resources, such as petroleum, coal, and natural gas, stand for the main suppliers of the global energy system, accounting for around 80% of primary energy consumption [1]. With the dwindling of oil reserves and the urgently growing demand for energy, along with increasing concerns about environmental pollution and greenhouse gas emissions, the transformation of renewable biomass into chemicals is attracting increasing attention from the scientific and industrial communities [2–4]. From this perspective, biomass as a raw material for the manufacture of chemicals (e.g., biodegradable polymers like polylactic acid) and as transport fuels is currently a central focus of research [5, 6]. Among these, the catalytic conversion of carbohydrates, which represent 75% of the annual renewable biomass [3, 7], can generate high added-value fuels and chemicals, such as 5-hydroxymethylfurfural (5-HMF). 5-HMF is a versatile molecular platform that can be produced by acid-catalyzed dehydrogenation of lignocellulose compounds [8]. 5-HMF is an alternative nonpetroleum precursor, which can be used as a chemical building block for the production of various high-volume organic chemicals aiming at numerous industrial applications. These chemicals include the 2,5-furandicarboxylic acid (FDCA) and 2,5-dimethylfuran (2,5-DMF), which can be used as biofuels [9–13]. 5-HMF is also regarded as an important precursor for the production of high added-value polymers such as polyurethanes, polyamides, and polyesters [14, 15].

✉ Benoît Champagne
benoit.champagne@unamur.be

[1] Laboratory of Organic Chemistry (LR17ES08), Faculty of Sciences, University of Sfax, 3038 Sfax, Tunisia

[2] Laboratory of Theoretical Chemistry, Theoretical and Structural Physical Chemistry Unit, NISM (Namur Institute of Structured Matter), University of Namur, rue de Bruxelles, 61, 5000 Namur, Belgium

Published online: 04 April 2022

In the recent years, the synthesis of bio-based polyethylene terephthalate (PET) has aroused a great interest. In fact, the petroleum route, which rests upon the polymerization reaction between ethylene glycol and terephthalic acid (TA), corresponds to the main source for obtaining PET. Currently, the synthesis of TA derives mainly from the liquid-phase oxidation of *p*-xylene (PX) originating from petroleum. However, worldwide efforts are being oriented to explore alternative pathways of TA and ethylene glycol from renewable biomass resources [16]. Among these, PX can be produced from the Diels–Alder (DA) cycloaddition reaction of 2,5-DMF with ethylene. Much research has been conducted on the process of synthesizing bio-based PX via this reaction [17–28]. The DA reaction is indeed one of the most useful synthetic reactions in organic chemistry, in which a diene (rich in electrons) adds to a dienophile (poor in electrons) forming a six-membered ring [29–31]. The process of bond breaking and bond formation in the DA reaction is considered concerted but not necessarily synchronous. In extreme cases, the DA reaction can even become a two-step process with a zwitterionic or a biradical intermediate. The DA reaction has been widely investigated experimentally as well as using quantum chemical modeling. In particular, frontier molecular orbital (FMO) theory and density functional theory (DFT) have been used to explain the reactivity, the reaction mechanism, and the selectivity of cycloaddition reactions [32–43].

Recently, using DFT with the M06-2X exchange–correlation functional (XCF), Nikbin et al. [17] have addressed the uncatalyzed and acid-catalyzed (Lewis and Brønsted) cycloadditions between 2,5-DMF and ethylene and the subsequent dehydration of the cycloadduct to produce PX. They modeled the Lewis acid (LA) sites of zeolites by bare alkali ions and the Bronsted site by a proton. They have demonstrated that i) only Lewis acids are able to catalyze the DA cycloaddition by reducing the HOMO–LUMO gap and therefore the activation barrier, ii) Li^+ is the strongest Lewis acid, and iii) both the Brønsted and Lewis acids can catalyze the dehydration reaction. Solvent effects were not considered in their work. Later on, Nikbin and co-workers have invested cluster models of the zeolite framework, showing that HY and alkaline-Y can catalyze the cycloaddition and dehydration reactions, and they highlighted that HY is much more efficient than alkaline-Y[18]. Using DFT (M06-2X XCF), Salavati-fard et al. explored the mechanism of the DA reaction between 2,5-DMF and maleic anhydride [44]. Reaction paths were reported for the uncatalyzed as well as the catalyzed (Lewis and Brønsted acids) reactions *in vacuo* and in a wide variety of solvents. Based on the activation barrier of the order of 24 kcal mol^{-1}, they concluded that the uncatalyzed Diels–Alder reaction is thermally feasible in vacuo, while LA (modeled as Na^+) reduces the activation barrier by interacting with maleic anhydride, which leads to a decrease of the HOMO(2,5-DMF)-LUMO(maleic anhydride) gap of the two reactants. With Brønsted acid (BA), one of the carbonyl oxygens of maleic anhydride is protonated, changing the reaction mechanism from concerted to stepwise and removing the activation barrier. Moreover, they found that increasing the polarity of solvents, as modeled with the SMD approach, makes the LA catalysis less efficient but brings the activation barriers of the both concerted and stepwise pathways closer together. Later, Rohling et al. [19] performed periodic DFT calculations on the DA reaction between 2,5-DMF and ethylene in low-silica alkali(M)-exchanged faujasites (MY; Si/Al = 2.4; $M^+ = Li^+$, Na^+, K^+, Rb^+, Cs^+). They reported that confinement leads to a destabilization of the reactants and a stabilization of the transition state (TS). Among the MY, the most significant reactant destabilization is found in RbY. Anti-bonding orbital interactions are found between the reactant and the cation, indicating that the TS stabilization arises from ionic interactions. In addition, RbY exhibits an optimal combination of confinement effects, resulting in having the lowest computed activation energy. They have also performed a mechanistic study on TM-[Cu(I), Cu(II), Zn(II), Ni(II), Cr(III), Sc(III), V(V)] exchanged faujasites to elucidate the effect of d-shell filling on the DA reaction between 2,5-DMF and ethylene [20]. Two pathways were established, one being the concerted one-step and the other being the stepwise two-step pathway. Their study has highlighted that a decrease in the d-shell filling brings about a concomitant increase of the reactant activation as evidenced by a smaller HOMO–LUMO gap and a lowering of the activation barrier. For models holding relatively small d-block cations, the zeolite framework was found to bias the DA reaction toward an asynchronous one-step pathway instead of the two-step pathway.

To rationalize DA reactions, Domingo et al. [45, 46] have proposed a polar mechanism, where the feasibility of the reaction depends on the nucleophilic and electrophilic characters of the diene and dienophile, respectively. They found a good correlation between experimental activation energies and the polar character of the cycloaddition as determined by the calculated charge transfer (CT) [using the natural bond order (NBO) method] at the corresponding TSs. This relationship has been further confirmed between B3LYP/6-31G(d) activation energies and these CT amplitudes, as well as between the activation energies and the electrophilicities of the substituted dienophiles. In this frame, because it is non-polar, as characterized by a negligible CT, the reaction between ethylene and butadiene presents a high activation energy (> 20 kcal/mol), so that it does not easily take place in the laboratory. On the other hand, the activation energy is reduced when the ethylene is substituted by electron withdrawing groups or when it complexes an LA, because the polarity of the reaction is enhanced [45–47].

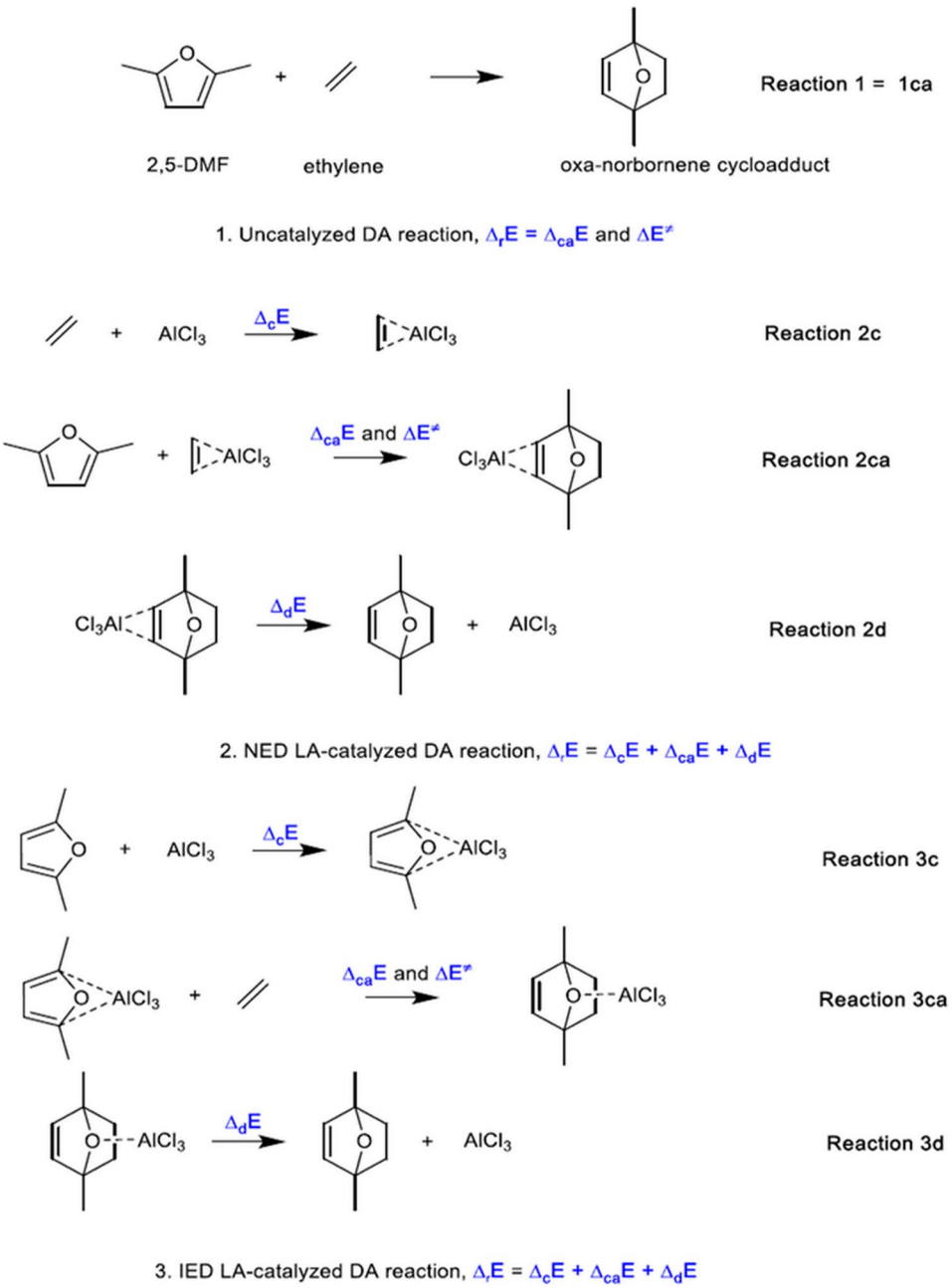

Scheme 1 Schematic representation of the uncatalyzed and LA-catalyzed DA reactions between 2,5-DMF and ethylene, key energies of reaction [cycloaddition (**ca**), activation ($\neq$), complexation (**c**), and decomplexation (**d**)], and equation labeling

In the present contribution, DFT is used to describe the uncatalyzed (Scheme 1.1) and LA-catalyzed DA reactions between 2,5-DMF and ethylene. $AlCl_3$ is selected as LA, because it is broadly used experimentally [48]. Two situations are tackled, i.e., when $AlCl_3$ is complexed either (i) by ethylene, which corresponds to the normal electron-demand (NED) DA reaction (Scheme 1.2) or (ii) by 2,5-DMF, which is known as the inverse electron-demand (IED) DA reaction (Scheme 1.3). These reactions are characterized both in vacuo and in solvents (1,4-dioxane, chloroform, and acetonitrile). In each case, structural, electronic, and thermochemical properties of the reactants, transition states, and products are predicted and interpreted. This work is organized as follows: the details on the computational procedure are portrayed in the next section, and the results are then displayed and discussed. Eventually, pertinent conclusions are drawn in the closing section.

2 Computational details

The equilibrium structures of the reactants, products, and transition states were optimized at the DFT level using the M06-2X XCF [49] and the 6–311 + G(d,p) basis set.

Vibrational frequencies were computed to confirm the stationary character of the reactants and products (no imaginary frequency) as well as transition states (one imaginary frequency). To assess the impact of selecting the M06-2X XCF, additional DFT calculations were performed using a selection of XCFs (M06 [49], M06L [50], M06HF [51], B3LYP [52, 53], and ωB97X-D [54]) and compared to reference results obtained at the coupled-cluster singles and doubles (CCSD) level of theory. Single-point aug-cc-pVDZ and aug-cc-pVTZ CCSD energies were calculated on geometries optimized at the MP2/6–311 + G(d,p) level. Additional single-point MP2 energies were also evaluated using the cc-pVDZ, cc-pVTZ, cc-pVQZ, aug-cc-pVDZ, and aug-cc-pVTZ basis sets [55] to highlight the effects of diffuse functions.

Departing from each transition states (TS), M06-2X/6–311 + G(d,p) calculations were performed to describe the structures and energies along the intrinsic reaction coordinate (IRC). For all species, reactants, products, and TS, the standard energy ($\Delta_r E$, $\Delta E^{\neq}$), enthalpy ($\Delta_r H°$, $\Delta H^{\neq}$), entropy ($\Delta_r S°$, $\Delta S^{\neq}$), and Gibbs enthalpy ($\Delta_r G°$, $\Delta G^{\neq}$) of both reaction and activation were evaluated. Solvent effects were modeled with the IEFPCM model [56]. Calculations were initially performed for $T = 298.15$ K and $P = 1.0$ atm. Then, a concentration correction of + 1.89 kcal mol^{-1} in the calculation of solvation free energies was used to account for the change of conditions when going from gas phase at 1 atm to solution at 1 M concentration [57]. This correction was also performed on the in vacuo values to better highlight the effects of the surrounding medium. This correction corresponds to a modification of the solvation entropies by − 6.34 cal mol^{-1} K^{-1}.

To evaluate the amplitude of the charge transfer between the reactants at the transition state, a natural bond orbital (NBO) analysis [58] was carried out. Following the approach of conceptual DFT (CDFT) [59–61], several descriptors of the electronic structure and reactivity were evaluated, including the energies of both the highest occupied molecular orbital (HOMO, ε_H) and the lowest unoccupied molecular orbital (LUMO, ε_L), the LUMO–HOMO gap (gap = ε_L—ε_H), the global electrophilicity ($\omega = \mu^2/2\eta$) [62], the chemical potential [$\mu = (\varepsilon_H + \varepsilon_L)/2$] [59], and the global hardness ($\eta = \varepsilon_L - \varepsilon_H$) [63]. According to Ref. [64], the nucleophilicity index (N) was calculated as $N = \varepsilon_H$ (Nu) − ε_H (TCE) where Nu is the nucleophile and TCE is the tetracyano-ethylene reference. In addition, the difference between the global electrophilicity indices of the reactants ($\Delta\omega = \omega_{diene} - \omega_{dienophile}$) [65] was evaluated, because it determines the polar character of the process. All calculations were carried out with the Gaussian09 software package [66].

3 Results and discussion

3.1 Assessment of the M06-2X XCF

This section centers around the calculation of the state functions by means of DFT with the different XCFs for the uncatalyzed and LA-catalyzed DA reactions between 2,5-DMF and ethylene in 1,4-dioxane (Scheme 1). The results are compared to reference CCSD values. The list of thermochemical data is provided in Tables S1 and S2 (Supplementary data). The corresponding energies of reaction and activation are plotted in Figs. 1 and 2. Note that Fig. 1 displays not only the $\Delta_r E$ of the DA cycloaddition but also the energies of complexation of $AlCl_3$ by ethylene and by 2,5-DMF as well as the energies of decomplexation of the products.

The correlation coefficients of the linear regressions with respect to the reference CCSD results are very good ($R > 0.98$), with the exception of B3LYP (both for the reaction and activation energies) and M06L (activation energies only). For the reaction energies (Fig. 1), the intercept at the origin is smaller than 1 kcal mol^{-1} for the M06-2X, M06, and ωB97X-D XCFs as well as for MP2, while the slopes are larger than one and slightly better with the M06 and ωB97X-D XCFs than with M06-2X and MP2. For the other XCFs (M06L, M06HF, and B3LYP), the intercept at the origin is larger and/or the slope deviates more substantially from one. For the activation energies (Fig. 2), the

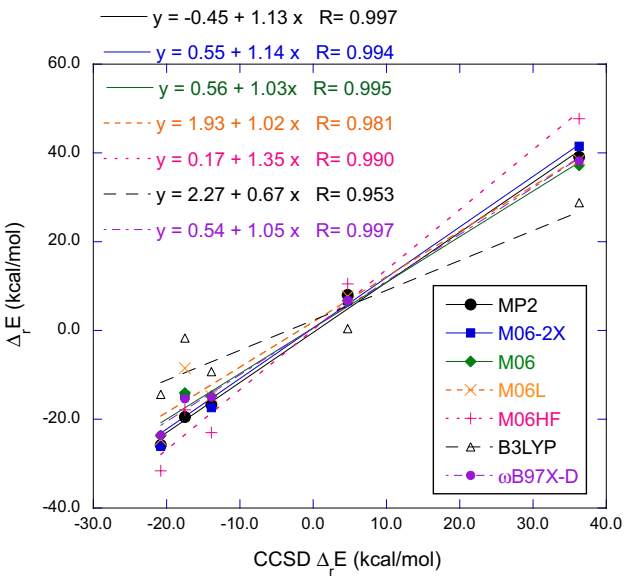

Fig. 1 Correlation between the energies of reaction, $\Delta_r E$ (**1ca**, **2c**, **3c**, **2d**, and **3d**), calculated at different levels of approximation (DFT with several XCFs as well as MP2) in comparison to reference CCSD results

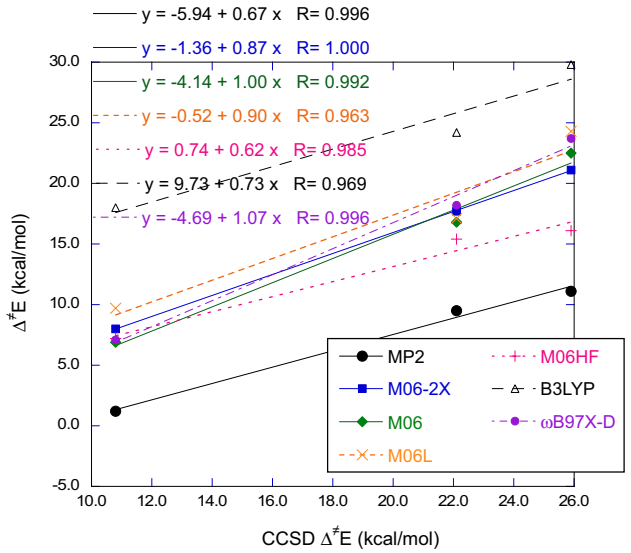

Fig. 2 Correlation between the energies of activation, $\Delta E^{\neq}$ (**1ca**, **2c**, **3c**, **2d**, and **3d**), calculated at different levels of approximation (DFT with several XCFs as well as MP2) in comparison to reference CCSD results

best slopes are obtained with the M06 (1.00) and ωB97X-D (1.07) XCFs, but the M06-2X slope (0.87) is also close to one, whereas its intercept at the origin is much smaller (− 1.4 kcal mol^{-1} versus − 4.1 and − 4.7 kcal mol^{-1} for M06 and ωB97X-D). M06L presents results in very good agreement with CCSD, whereas M06HF, B3LYP, and MP2 perform poorly. As a matter of fact, the choice of M06-2X as reliable XCF to study these (catalyzed) DA reactions is justified, keeping in mind that it systematically underestimates the variations of activation energies.

3.2 Analysis of the CDFT reactivity indices of the reactants

Using the optimized geometrical structures, the CDFT descriptors of the reactants in vacuo and in solution were calculated (Table S3), which sets forward a first analysis of their reactivity. The chemical potential of 2,5-DMF ($\mu = -3.4$ eV) is larger than that of ethylene ($\mu = -4.2$ eV), confirming the transfer of electron from 2,5-DMF to ethylene. This is also consistent with (i) the HOMO energy of 2,5-DMF (from − 7.1 eV to − 7.3 eV as a function of the solvent) higher than that of ethylene (from − 9.1 eV to − 9.2 eV), (ii) the electrophilicity index of ethylene (0.9 eV) slightly larger than that of 2,5-DMF (0.8 eV), (iii) the nucleophilicity index of the 2,5-DMF (in vacuo, 3.8 eV) larger than that of ethylene (in vacuo, 1.8 eV), and (iv) the smaller value of ΔE (NED) = [ε_L (ethylene)—ε_H (2,5-DMF) = 7.8 eV] with respect to ΔE(IED) = [ε_L (2,5-DMF)—ε_H (ethylene) = 9.5 eV]. This indicates a preference of interaction between the HOMO of the 2,5-DMF and the LUMO of the ethylene (Fig. 3, Figs. S1, S2, and S3), which is in good agreement with the frontier molecular orbital (FMO) theory [32]. In addition, 2,5-DMF is a weak electrophile ($\omega = 0.8$ eV) and a strong nucleophile (N from 3.2 to 3.8 eV), while ethylene is also classified as a weak electrophile ($\omega = 0.9$ eV) and a rather weak nucleophile (N from 1.3 to 1.8 eV) according to the electrophilicity and nucleophilicity [67] scales. Yet, the aromaticity of 2,5-DMF is a detrimental factor to its nucleophilicity, but the presence of the two methyl groups is enhancing it. Indeed, N(furan) = 3.0 eV and N(cyclopentadiene) = 3.4 eV in comparison to 3.8 eV for 2,5-DMF. Thus, the uncatalyzed DA reaction has a low polar character, further characterized by the low value of the difference of electrophilicity index between the two reactants ($\Delta\omega = 0.1$ eV).

The coordination of $AlCl_3$ with 2,5-DMF and ethylene stabilizes the energy of their frontier orbitals. Therefore, the coordination of $AlCl_3$ with ethylene increases its electrophilicity (in vacuo, $\omega = 1.8$ eV versus 0.9 eV) and decreases its nucleophilicity (in vacuo, $N = 0.3$ eV versus 1.8 eV). Combining the strong electrophilic character of the ethylene–$AlCl_3$ complex with the strong nucleophilic character of 2,5-DMF (in vacuo, $N = 3.8$ eV) makes that the NED LA-catalyzed DA reaction will have a very polar character ($\Delta\omega = -1.0$ eV). This is accompanied by a reduction of the HOMO–LUMO gap, ΔE(NED) = [ε_L(ethylene-$AlCl_3$)—ε_H (2,5-DMF)] which, in vacuo, goes down to 5.8 eV versus 7.8 eV for the uncatalyzed reaction. On the other hand, $AlCl_3$ better stabilizes the HOMO of 2,5-DMF than its LUMO, decreasing its donor character (in vacuo, N = 2.1 eV versus 3.8 eV) while increasing its acceptor character (in vacuo, $\omega = 1.4$ eV versus 0.8 eV), so that the polar character of the reaction is also increased, through it is opposite to the previous situation. Indeed, in this case, the IED reaction is favored with ΔE(IED) = [ε_L(2,5-DMF-$AlCl_3$)—ε_H (ethylene)] = 8.4 eV in vacuo (Fig. 3), but this difference of FMO energies is larger than for the uncatalyzed NED reaction, which results mostly from the weak nucleophilic character of ethylene. This comparison between the different mechanisms of $AlCl_3$ complexation demonstrates that $AlCl_3$ further promotes the NED LA-catalyzed DA reaction. Moreover, for both the uncatalyzed and the LA-catalyzed DA reactions, and for the different diene/dienophile combinations, the FMO gaps increase slightly with the polarity of the solvent (Fig. S4).

3.3 Thermodynamic analysis

This section is devoted to the M06-2X/6–311 + G(d,p) calculation of the thermochemical state functions for the uncatalyzed and LA-catalyzed DA reactions between 2,5-DMF and ethylene in vacuo and in various solvents (1,4-dioxane, chloroform, and acetonitrile). The reaction and activation

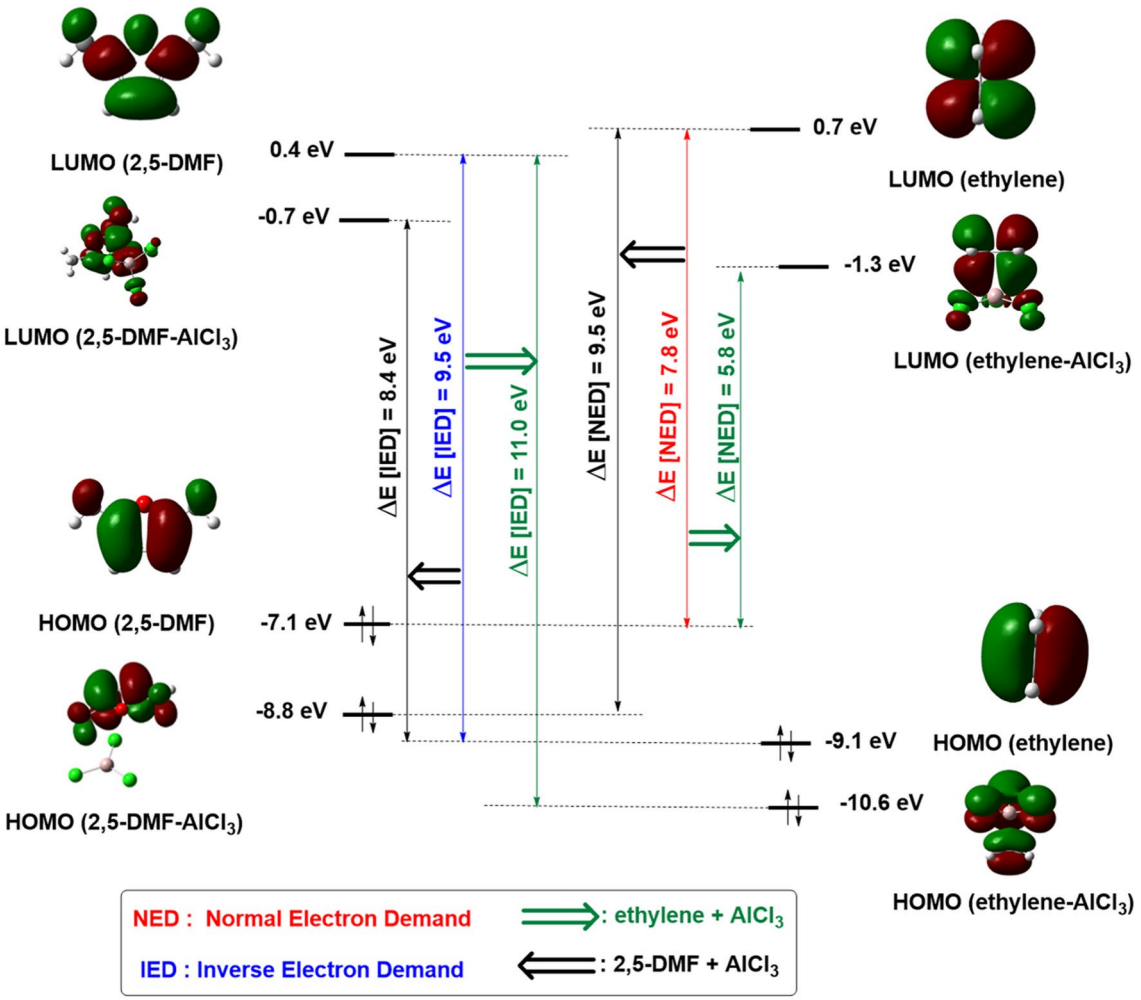

Fig. 3 Frontier molecular orbital diagram of the uncatalyzed and LA-catalyzed DA reactions between 2,5-DMF and ethylene, the electronic structures and energies were calculated at the M06-2X/6–311 + G(d,p) level in vacuo

energies are summarized in Table 1, while the individual values for the reactants, products, and TSs are given in Table S4 (Supporting Information).

Table 1 reveals that the DA reaction between 2,5-DMF and ethylene is exothermic ($\Delta_r H° < 0$), but slightly endergonic ($\Delta_r G° > 0$). The solvent has a minor impact on Δ_rH°, on Δ_rG° (reduction from 0.1 to 0.3 kcal mol^{-1}), and on Δ_rS° (increase from 0.2 to 0.8 cal mol^{-1} K^{-1}). Likewise, the activation barrier of the uncatalyzed DA reaction unveils a modest influence of the solvent, increasing by less than 0.5 kcal mol^{-1} across the range of displayed examples (Fig. 4). Yet, the uncatalyzed DA reaction between 2,5-DMF and ethylene exhibits a high activation energy ($\Delta G^{\neq}$ ~35 kcal mol^{-1}). This large activation barrier, associated with the non-polar character of the reaction of the uncatalyzed cycloaddition, is responsible for the absence of reaction in the laboratory [17].

On the other side, for the NED LA-catalyzed DA reaction (complexation of $AlCl_3$ with ethylene, Scheme 2), $AlCl_3$ leads to a strong decrease of the activation barrier ($\Delta\Delta G^{\neq} = \Delta G^{\neq}$(**1ca**) – $\Delta G^{\neq}$(**2ca**) = 9.2 kcal mol^{-1} in gas phase, 11.4 kcal mol^{-1} in 1,4-dioxane, 12.3 kcal mol^{-1} in chloroform, and 12.6 kcal mol^{-1} in acetonitrile). For the IED LA-catalyzed DA reaction (complexation of $AlCl_3$ with 2,5-DMF, Scheme 3), a smaller decrease of $\Delta G^{\neq}$ is observed ($\Delta\Delta G^{\neq} = \Delta G^{\neq}$(**1ca**) – $\Delta G^{\neq}$(**3ca**) = 3.3 kcal mol^{-1} in gas phase, 5.2 kcal mol^{-1} in 1,4-dioxane, 6.9 kcal mol^{-1} in chloroform, and 8.3 kcal mol^{-1} in acetonitrile). Moreover, for both mechanisms of the LA-catalyzed DA reaction, the largest decrease in the activation barrier is reported for acetonitrile (Fig. 4). This highlights that by increasing the polarity of the solvents, the catalytic power of $AlCl_3$ increases.

Table 2 discloses the values of the thermodynamic quantities of LA complexation and decomplexation reactions for both modes of coordination (Reactions **2c**, **3c**,

2d, and **3d**, Scheme 1), in vacuo and in solution (1,4-dioxane, chloroform, and acetonitrile). The LA complexation reaction is exothermic [$\Delta_c H°(\mathbf{2c/3c}) < 0$] and exergonic [$\Delta_c G°(\mathbf{2c/3c}) < 0$] in vacuo and in solution. In parallel, the LA decomplexation reaction is endothermic [$\Delta_d H°(\mathbf{2d/3d}) > 0$], but exergonic [$\Delta_r G°(\mathbf{2d}) < 0$] for the NED mechanism and endergonic [$\Delta_d G°(\mathbf{3d}) > 0$] for the IED mechanism. The complexation is stronger in the case of 2,5-DMF [$\Delta_c X(\mathbf{3c}) < \Delta_c X(\mathbf{2c})$, with $X = E$, $H°$, and $G°$]. Therefore, the corresponding decomplexation is also more difficult [$\Delta_d X(\mathbf{3d}) > \Delta_d X(\mathbf{2d})$], which refers to the formation of a strong coordinating bond between the oxygen atom and $AlCl_3$. This is indicative that the IED LA-catalyzed DA reaction is less favorable than the NED LA-catalyzed DA reaction, because the complex is more stabilized, leading to larger effective activation barriers.

Combining these different reactions, the relative Gibbs free energy diagrams of the uncatalyzed and LA-catalyzed DA reactions between 2,5-DMF and ethylene in vacuo and in solution (1,4-dioxane, chloroform, and acetonitrile) are displayed in Figs. 5, 6, 7 and 8, respectively. For the uncatalyzed process, the TS energy relative to those of the isolated reactants amounts to 34.7 kcal mol^{-1} in vacuo, 34.9 kcal mol^{-1} in 1,4-dioxane, 35.0 kcal mol^{-1} in chloroform, and 35.1 kcal mol^{-1} in acetonitrile. Then, for the catalyzed reaction, where $AlCl_3$ is complexed by ethylene (NED), the energy difference between the reactants and the TS is 20.1 kcal mol^{-1} (in vacuo), 18.4 kcal mol^{-1} (in 1,4-dioxane), 16.9 kcal mol^{-1} (in chloroform), and 15.8 kcal mol^{-1} (in acetonitrile). On the other hand, the activation free enthalpy with respect to the ethylene–$AlCl_3$ complex attains 27.3, 25.5, 24.6, and 24.4 kcal mol^{-1} for the environments given in the same order. Proceeding in the same way, for the IED process (the $AlCl_3$ is complexed by 2,5-DMF), the TS energies difference between the reactants and the TS attains 20.3 kcal mol^{-1} (in vacuo), 18.8 kcal mol^{-1} (in 1,4-dioxane), 17.0 kcal mol^{-1} (in chloroform), and 15.3 kcal mol^{-1} (in acetonitrile). Again, the values are larger when considering the complexation of $AlCl_3$ by 2,5-DMF: 33.3, 31.6, 30.0, and 28.7 kcal mol^{-1}, respectively. In summary, the reaction is facilitated by the attachment of $AlCl_3$ and by increasing the polarity of solvent, with the NED LA-catalyzed reaction being more favorable than the IED LA-catalyzed reaction. Yet, the 2,5-DMF–$AlCl_3$ complex is preferentially formed, but the ΔG° difference with respect to the complexation of $AlCl_3$ by ethylene, ranging between 5 and 6 kcal mol^{-1} as a function of the solvent, demonstrates that there is an equilibrium between the two types of complexes.

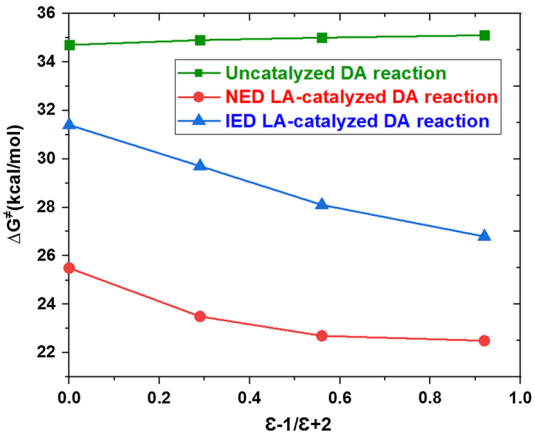

Fig. 4 Variation of the free enthalpy of activation for the uncatalyzed and LA-catalyzed DA reactions plotted as a function of solvent polarity, represented by the $\varepsilon - 1/\varepsilon + 2$ function

Table 1 Thermochemical state functions ($\Delta_r E$, $\Delta_r H°$, $\Delta_r G°$, $\Delta E^{\neq}$, $\Delta H^{\neq}$, $\Delta G^{\neq}$ in kcal mol^{-1} and $\Delta_r S°$, $\Delta S^{\neq}$ in cal mol^{-1} K^{-1}) of the uncatalyzed and LA-catalyzed DA reactions between 2,5-DMF and ethylene at the M06-2X/6–311 + G(d,p) level

	Reactions	$\Delta_r E$	$\Delta_r H°$	$\Delta_r G°$	$\Delta_r S°$	$\Delta E^{\neq}$	$\Delta H^{\neq}$	$\Delta G^{\neq}$	$\Delta S^{\neq}$
In vacuo	**1ca**	− 14.8	− 12.0	2.3	− 47.8	20.8	21.5	34.7	− 44.2
	2ca					10.0	10.8	25.5	− 49.3
	3ca					19.2	19.7	31.4	− 39.2
1,4-dioxane ($\varepsilon = 2.25$)	**1ca**	− 14.7	− 11.9	2.3	− 47.6	21.1	21.8	34.9	− 45.0
	2ca					8.0	8.9	23.5	− 49.1
	3ca					17.8	18.3	29.7	− 38.2
Chloroform ($\varepsilon = 4.81$)	**1ca**	− 14.7	− 11.9	2.2	− 47.3	21.3	22.0	35.0	− 43.7
	2ca					7.1	8.1	22.7	− 49.0
	3ca					16.7	17.2	28.1	− 36.5
Acetonitrile ($\varepsilon = 37.5$)	**1ca**	− 14.9	− 12.0	2.0	− 47.0	21.4	22.2	35.1	− 43.4
	2ca					6.5	7.5	22.5	− 50.1
	3ca					15.6	16.1	26.8	− 36.2

Solvents (1,4-dioxane, chloroform, and acetonitrile) effects were described using IEFPCM

Table 2 Thermochemical state functions of LA complexation and decomplexation reactions ($\Delta_{c/d}E$, $\Delta_{c/d}H°$, $\Delta_{c/d}G°$, in kcal mol^{-1} and $\Delta_{c/d}S°$ in cal mol^{-1} K^{-1}) at the M06-2X/6–311 + G(d,p) level

	Reactions	$\Delta_{c/d}E$	$\Delta_{c/d}H°$	$\Delta_{c/d}G°$	$\Delta_{c/d}S°$
In vacuo	**2c**	− 16.5	− 15.0	− 7.2	− 26.2
	2d	6.6	5.5	− 2.4	26.4
	3c	− 25.3	− 23.9	− 13.0	− 36.4
	3d	40.6	38.7	28.5	34.3
1,4-Dioxane (ε = 2.25)	**2c**	− 17.4	− 15.9	− 7.1	− 29.8
	2d	6.7	5.6	− 2.9	27.7
	3c	− 26.1	− 24.6	− 12.8	− 39.6
	3d	41.5	39.7	28.4	36.9
Chloroform (ε = 4.81)	**2c**	− 18.0	− 16.5	− 7.7	− 29.7
	2d	6.5	5.5	− 2.4	26.7
	3c	− 26.5	− 25.0	− 13.0	− 40.3
	3d	42.0	40.2	28.9	38.3
Acetonitrile (ε = 37.5)	**2c**	− 18.6	− 17.1	− 8.6	− 28.7
	2d	2.2	1.1	− 4.5	18.7
	3c	− 27.0	− 25.5	− 13.4	− 40.5
	3d	42.5	40.6	29.3	37.9

Solvents (1,4-dioxane, chloroform, and acetonitrile) effects were described using IEFPCM

3.4 Impact of the dimerization of $AlCl_3$ and other coordination reactions involving $AlCl_3$

$AlCl_3$ is known to dimerize. The dimerization data are provided in Table 3 for the reactions in vacuo and in solution. The $AlCl_3$ dimerization reaction has exothermic and exergonic characters. Thus, during this reaction, the formation of Al_2Cl_6 dimer is favored. This has an impact on the amount of $AlCl_3$ that can act as a LA catalyst with either of the reactant. Therefore, if considering the reaction between the Al_2Cl_6 dimer and ethylene, the formation of the ethylene-$AlCl_3$ complex is characterized by ΔG° of 4.1 kcal mol^{-1} of ethylene in vacuo but only 0.3 kcal mol^{-1} in acetonitrile. This demonstrates that if the solvent is polar enough, the complex is formed in sufficient amount, leading to an activation barrier of ~ 16 kcal mol^{-1}. Similarly, the formation of the 2,5-DMF-$AlCl_3$ complex from the Al_2Cl_6 dimer has a ΔG° of − 1.7 kcal mol^{-1} in vacuo and − 4.5 kcal mol^{-1} in acetonitrile. Therefore, in acetonitrile, the activation barrier amounts to ~ 20 kcal mol^{-1}.

Considering the complex between the product and $AlCl_3$, if the interaction occurs with the CC double bond, the stabilization is weak so that it easily dissociates to get the DA product and $AlCl_3$, and even more easily Al_2Cl_6. In the latter case, the resulting $\Delta_d G°$ values amount to about − 13 kcal mol^{-1}. On the other hand, if the interaction occurs with the O atom, the complex is better stabilized, with dissociation free energies ranging, as a function of the medium,

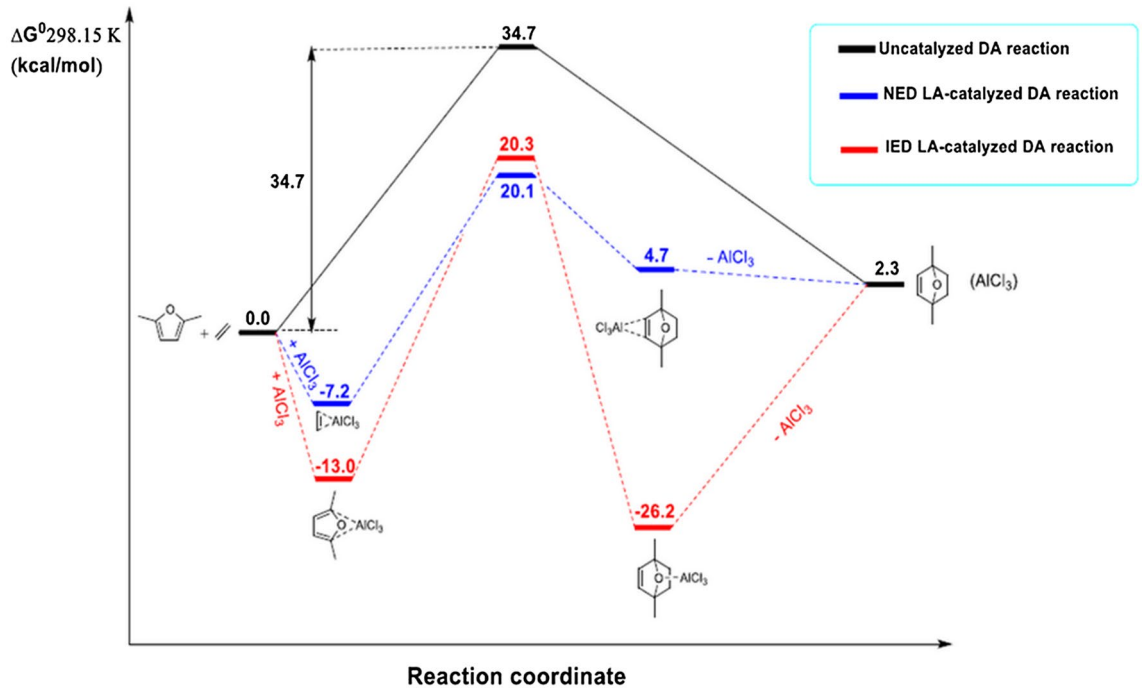

Fig. 5 Relative Gibbs free energy diagram of the uncatalyzed and LA-catalyzed DA reactions between 2,5-DMF and ethylene in vacuo at the M06-2X/6–311 + G(d,p) level

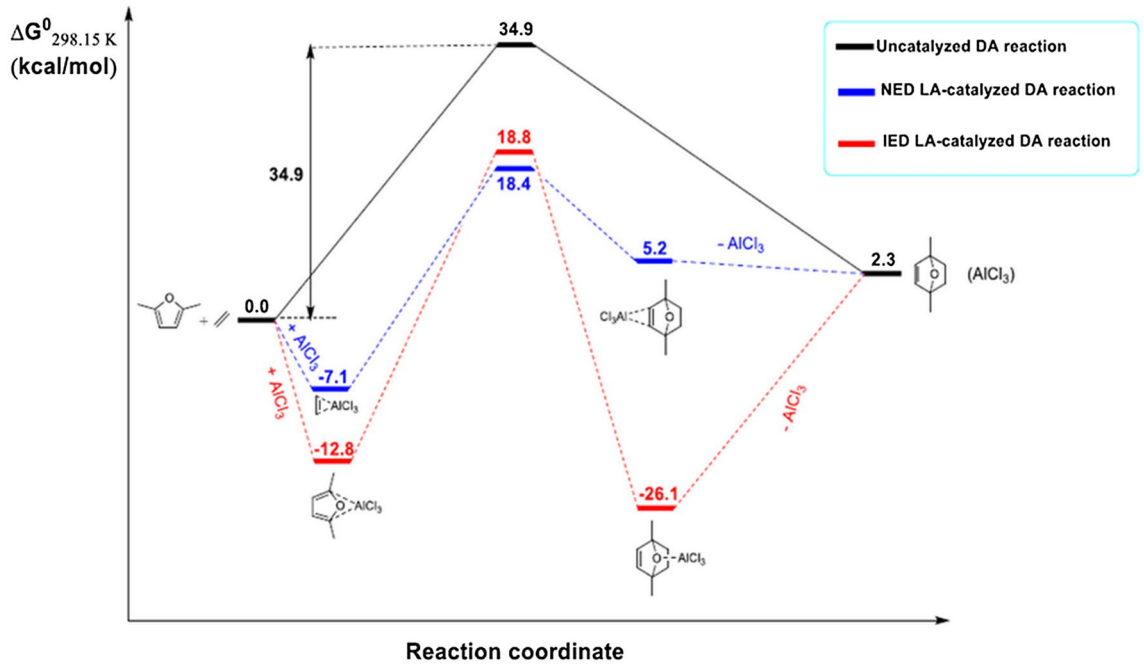

Fig. 6 Relative Gibbs free energy diagram of the uncatalyzed and LA-catalyzed DA reactions between 2,5-DMF and ethylene at the [IEFPCM (1,4-dioxane)/M06-2X/6-311G + (d,p)] level

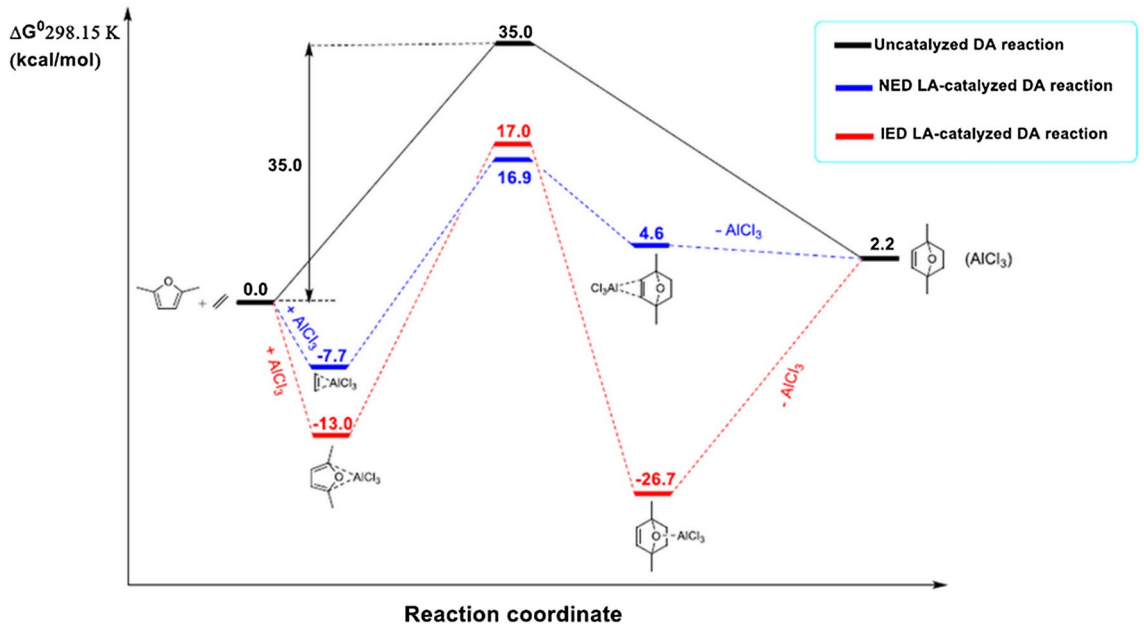

Fig. 7 Relative Gibbs free energy diagram of the uncatalyzed and LA-catalyzed DA reactions between 2,5-DMF and ethylene at the [IEFPCM (chloroform)/M06-2X/6-311G + (d,p)] level

from 28.5 to 29.3 kcal mol^{-1} when considering the liberation of $AlCl_3$ and from 17.2 to 20.4 kcal mol^{-1} when considering $AlCl_3$ molecules form dimers. Note that the addition of Lewis base can be used to displace the equilibrium of formation of the complexes between the product and $AlCl_3$ as evidenced in the case of Ziegler–Natta polymerizations

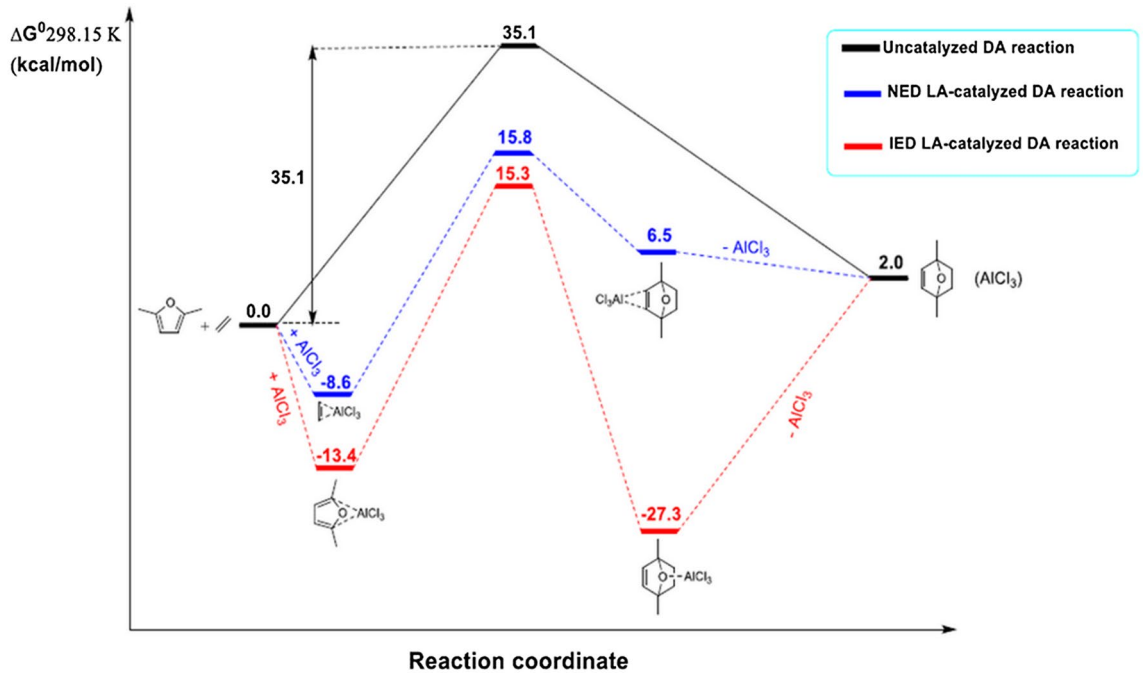

Fig. 8 Relative Gibbs free energy diagram of the uncatalyzed and LA-catalyzed DA reactions between 2,5-DMF and ethylene at the [IEFPCM (acetonitrile)/M06-2X/6-311G + (d,p)] level

Table 3 Thermochemical state functions ($\Delta_{dim}E$, $\Delta_{dim}H°$, and $\Delta_{dim}G°$ in kcal mol^{-1} and $\Delta_{dim}S°$ in cal mol^{-1} K^{-1}) of the $AlCl_3$ dimerization reaction calculated at the M06-2X/6–311 + G(d,p) level

	$2AlCl_3 \rightleftharpoons Al_2Cl_6$			
	$\Delta_{dim}E$	$\Delta_{dim}H°$	$\Delta_{dim}G°$	$\Delta_{dim}S°$
In vacuo	− 31.7	− 30.5	− 22.5	− 27.1
1,4-Dioxane ($\varepsilon = 2.25$)	− 30.6	− 29.4	− 19.6	− 33.1
Chloroform ($\varepsilon = 4.81$)	− 30.0	− 28.8	− 18.7	− 33.9
Acetonitrile ($\varepsilon = 37.5$)	− 29.4	− 28.2	− 17.7	− 35.4

Solvents (1,4-dioxane, chloroform and acetonitrile) effects were described using IEFPCM

where related organoaluminium co-catalysts are employed [68, 69].

Though one of the objectives of this work is to analyze the polarization effects of the solvent on the thermodynamics and kinetics of the DA reaction between 2,5-DMF and ethylene when catalyzed by an LA, one should notice that the LA has the ability to be complexed by the solvent molecules, as a function of their nature, i.e., their Lewis basicity. As shown in Table S5, this is particularly true for 1,4-dioxane and acetonitrile, for which the complexation is strongly exothermic and exergonic ($\Delta_c G° = -29.4$ and -26.3 kcal mol^{-1}, respectively). As a matter of fact, the Lewis acidity of $AlCl_3$ is quenched in these solvents, owing to the formation of a stable coordination bond between either the N atom (acetonitrile) or the O atom (1,4-dioxane) and $AlCl_3$. On the other hand, the Gibbs enthalpy of complexation of $AlCl_3$ by chloroform is almost zero, demonstrating that $AlCl_3$ is not displaced from its dimer by chloroform, and that $AlCl_3$ can catalyze the DA reaction.

Note that in the reaction path where $AlCl_3$ activates 2,5-DMF, one may wonder whether the most favorable coordination corresponds to the situation described above (Al coordinated by the aromatic ring, and linked to the C3 and C6 atoms) or rather to the situation where the furan oxygen complexes $AlCl_3$. Calculations performed at the same level of approximation demonstrate that the latter coordination mode is less favorable by about 4 kcal mol^{-1} (Table S6).

3.5 Geometries of transition states

The geometries of TSs for the uncatalyzed and LA-catalyzed DA reactions, for both modes of coordination (Scheme 1) are depicted in Fig. 9 together with the C_1–C_3 and C_2–C_6 bond lengths (nomenclature is shown in Schemes 2 and 3). For the uncatalyzed DA reactions, the lengths of the C_1–C_3 and C_2–C_6 forming bonds at the TSs are equal. Thus, the two σ bonds are formed at the same time and the cycloaddition takes place via a one-step synchronous mechanism. The lengths of the C–C bonds involved in the uncatalyzed DA process rise slightly by increasing the polarity of the solvents. On the other side, for the catalyzed processes, there is a degree of asynchronicity, which can be evaluated as

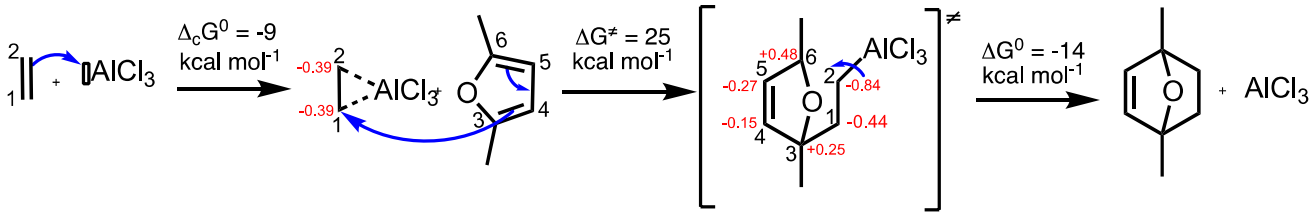

Scheme 2 Reaction mechanism of the NED LA-catalyzed DA reaction between 2,5-DMF ethylene together with geometric electronic, and thermodynamical quantities evaluated at the IEFPCM (acetonitrile)/M06-2X/6-311G + (d,p) level. Free energies are in kcal mol^{-1}

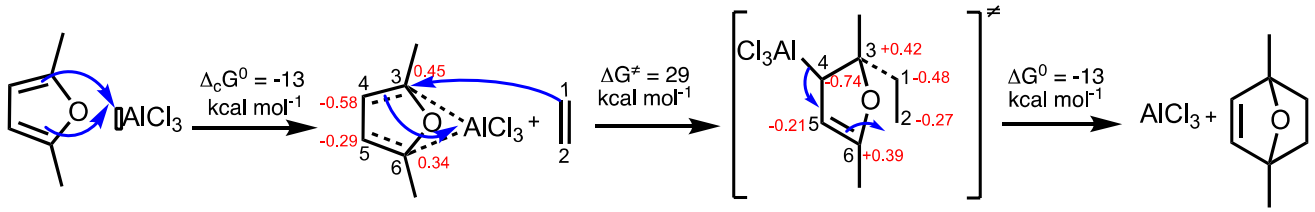

Scheme 3 Reaction mechanism of the IED LA-catalyzed DA reaction between 2,5-DMF and ethylene together with geometric, electronic, and thermodynamical quantities evaluated at the IEFPCM (acetonitrile)/M06-2X/6-311G + (d,p) level. Free energies are in kcal mol^{-1}

the difference between the C_1–C_3 and C_2–C_6 bond lengths, namely $\Delta d = d(C_2–C_6)—d(C_1–C_3)$. Their Δd values range between 0.425 and 0.576 Å for the NED process and between 0.435 and 0.527 Å for the IED process. In acetonitrile (and chloroform), this indicates that the NED process is more synchronous than the IED process, while the opposite is observed in vacuo and in 1,4 dioxane. Indeed, as the polarity of the solvent increases, the degree of asynchronicity decreases for the NED mechanism and increases for the IED mechanism. In the same order, the analysis of the vibrational normal coordinate corresponding to the unique imaginary vibrational frequency of the TSs (see the corresponding values in Fig. 9) indicates that they mainly concern the motion of the C_1, C_3, C_2, and C_6 atoms along the C_1–C_3 and C_2–C_6 bond formation.

Following the approach adopted in Refs. [70, 71], the amount of CT at the transition state was evaluated. q_{CT}(TS) is obtained as the sum of the natural atomic charge of the atoms belonging to the ethylene (uncatalyzed or IED LA-catalyzed reactions) or to the ethylene–$AlCl_3$ (NED LA-catalyzed reaction) moieties. Therefore, since the global charge of the ethylene/ethylene-$AlCl_3$ reactants is zero, a negative q_{CT}(TS) value corresponds to a transfer of charge from the 2,5-DMF-$AlCl_3$/2,5-DMF to ethylene/ethylene-$AlCl_3$ (NED), while a positive value to a IED mechanism. For the uncatalyzed DA reaction, q_{CT}(TS) values are − 0.06 e (in vacuo) and − 0.07 e (in 1,4-dioxane, chloroform, and acetonitrile), indicating the expected negligibly polar character of this cycloaddition, in agreement with the analysis of the CDFT indices (small Δω, large HOMO–LUMO gap, small electrophilicity of ethylene). Then, turning to the LA-catalyzed DA reaction, the calculated q_{CT}(TS) amounts to -0.43 e (in vacuo and in all the solvents) for the NED mechanism, highlighting a large electronic CT from 2,5-DMF to the ethylene–$AlCl_3$ complex (Fig. 9). This corresponds to a polar reaction, in agreement with a larger Δω value, a smaller HOMO–LUMO gap, and an increased electrophilicity of the dienophile with respect to the uncatalyzed reaction. On the other hand, for the IED mechanism, the amount of CT depends on the solvent and ranges from 0.08 e in vacuo, to 0.12 e in 1,4-dioxane, to 0.14 e in chloroform, and to 0.16 e in acetonitrile. The amount and direction of CT is consistent with the MO energies as well as with the sign of Δω.

Considering these geometries and the NBO population analysis, the following mechanisms can be disclosed. For the NED reaction, the formation of the C_2–$AlCl_3$ coordination bond creates an electrophilic site on the C_1 atom of ethylene (Scheme 2). This leads to a first nucleophilic attack resulting in the formation of the C_1–C_3 σ bond. This results in a transition state where the C_6 atom is electrophilic (in acetonitrile, $q = 0.48$ e), while C_2 is nucleophilic ($q = -0.84$ e). Then, C_2 reacts with C_6 to form the second σ bond. For the EID process, an electrophilic center is formed on the C_3 atom of 2,5-DMF owing to the formation of the C_4–$AlCl_3$ coordination (Scheme 3). It induces the electrophilic attack by any of the C atoms of ethylene to reach the transition state, which is characterized by the first σ bond in formation (C_1–C_3). In the IED transition state, the NBO charges on C_2 and C_6 amount to − 0.27 e and 0.39 e, respectively, leading to a favorable electrostatic interaction and the formation of the second σ bond.

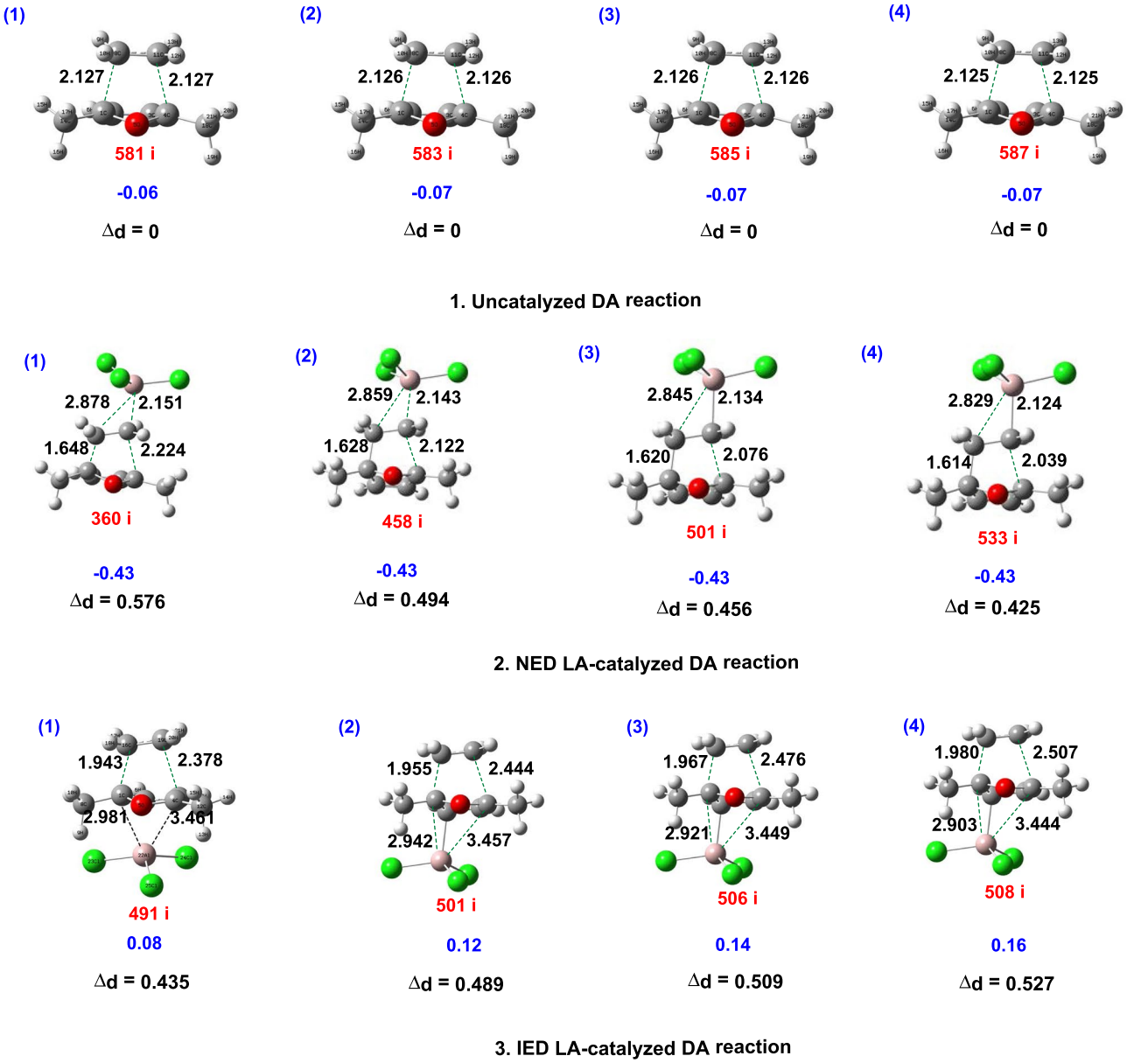

Fig. 9 Geometries of the TSs involved in the uncatalyzed and LA-catalyzed DA reactions between 2,5-DMF and ethylene. The distances and the Δd values are given in Å. The unique imaginary frequencies (red, cm^{-1}) are provided as well as the q_{CT} amplitudes at the TS with respect to the reactant (blue, e) [(1): in vacuo, (2):1,4-dioxane, (3):chloroform, and (4):acetonitrile]

4 Conclusion

The uncatalyzed and Lewis acid (LA)-catalyzed Diels–Alder reaction between 2,5-DMF and ethylene has been investigated using density functional theory (DFT). The uncatalyzed reaction is characterized by a large activation barrier ($\Delta G^{\neq} = 35$ kcal mol^{-1}). This corresponds to a normal electron-demand (NED) mechanism where ethylene is an electron acceptor whereas 2,5-DMF plays the role of electron donor. In other words, with the FMO scheme, an electron is promoted from the HOMO of 2,5-DMF to the LUMO of ethylene, whereas in the inverse electron-demand (IED) mechanism, the HOMO of ethylene interacts with the LUMO of 2,5-DMF. Moreover, adopting the tools of conceptual DFT, this reaction is shown to have a low polar character, as substantiated by a small difference of electrophilicity (0.1 eV) between the reactants as well as by a small electron charge transfer (CT) at the transition state (− 0.06 e, in vacuo). As a matter of fact, the effect of the solvent is negligible on the barrier of activation. In addition, the analysis of the geometrical structure of the transition state shows that the reaction takes place via a one-step synchronous process.

For the catalyzed reaction, $AlCl_3$ has been selected as LA. When it interacts with ethylene, forming a π-complex, it enhances its acceptor character, further favoring the NED over the IED mechanism. This is accompanied by a reduction of the free energy of the transition state. Therefore, the strong electrophilic character of the ethylene–$AlCl_3$ complex combined with the strong nucleophilic character of 2,5-DMF leads to a polar reaction pathway, which whom the activation barrier decreases with the solvent polarity. On the other hand, when $AlCl_3$ is complexed by 2,5-DMF, the IED mechanism is favored over the NED one, the polar character is slightly larger than for the uncatalyzed reaction, while a similar reduction of $\Delta G^{\neq}$ with the solvent polarity is observed. In addition, when the reaction is catalyzed, the two bonds formed at the TSs occur via a one-step asynchronous process. Moreover, the calculations have unraveled that the LA plays additional roles, i.e., (i) it forms stable complexes with any of the reactants, so that the increase of the activation barrier amounts to 9–12 kcal mol^{-1} for the NED mechanism and to 3–9 kcal mol^{-1} for the IED one, (ii) then, its complexes formed with the product can prevent the release of the latter, and finally, (iii) $AlCl_3$ forms dimers, which also impact the different equilibria. This paper paves therefore the way toward a better understanding of the reactivity and therefore valorization of 2,5-DMF, which is a direct product of biomass transformation. Forthcoming studies of our groups will tackle the Diels–Alder reaction with more elaborated dienophiles, such as acrolein.

The DFT calculations and analyses have been enacted by employing the M06-2X exchange-correlation functional, because, among a small set of functionals covering a broad range of Hartree–Fock exchange percentages, it better reproduces the reference reaction and activation energies evaluated using the coupled-cluster singles and doubles method.

Supplementary Information The online version contains supplementary material available at https://doi.org/10.1007/s00214-022-02880-y.

Acknowledgements The authors are grateful to the Ministry of Higher Education and Scientific Research of Tunisia, which financially supported this work. M.C. is grateful to UNamur for financially contributing to his research stay. The calculations were performed on the computers of the « Consortium des équipements de Calcul Intensif (CÉCI) » (http://www.ceci-hpc.be), including those of the « UNamur Technological Platform of High-Performance Computing (PTCI) » (http://www.ptci.unamur.be), for which we gratefully acknowledge the financial support from the FNRS-FRFC, the Walloon Region, and the University of Namur (Conventions No. 2.5020.11, GEQ U.G006.15, U.G018.19, 1610468, and RW/GEQ2016).

References

1. Briefing US (2013) International Energy Outlook. US Energy Information Administration
2. Huber GW, Iborra S, Corma A (2006) Chem Rev 106:4044–4098
3. Alonso DM, Bond JQ, Dumesic JA (2010) Green Chem 12:1493–1513
4. Mettler MS, Vlachos DG, Dauenhauer PJ (2012) Energy Environ Sci 5:7797–7809
5. Schmidt LD, Dauenhauer PJ (2007) Nature 447:914–915
6. Tong X, Ma Y, Li Y (2010) Appl Catal A 385:1–13
7. West RM, Kunkes EL, Simonetti DA, Dumesic JA (2009) Catal Today 147:115–125
8. Nikolla E, Román-Leshkov Y, Moliner M, Davis ME (2011) ACS Catal 1:408–410
9. Xia H, Xu S, Hu H, An J, Li C (2018) RSC Adv 8:30875–30886
10. Hu L, Tang X, Xu J, Wu Z, Lin L, Liu S (2014) Ind Eng Chem Res 53:3056–3064
11. Kumalaputri AJ, Bottari G, Erne PM, Heeres HJ, Barta K (2014) Chemsuschem 7:2266–2275
12. Iriondo A, Mendiguren A, Güemez MB, Requies J, Cambra JF (2017) Catal Today 279:286–295
13. Casanova O, Iborra S, Corma A (2009) Chemsuschem 2:1138–1144
14. Pacheco JJ, Labinger JA, Sessions AL, Davis ME (2015) ACS Catal 5:5904–5913
15. Pacheco JJ, Davis ME (2014) Proc Natl Acad Sci USA 111:8363–8367
16. Pang J, Zheng M, Sun R, Wang A, Wang X, Zhang T (2016) Green Chem 18:342–359
17. Nikbin N, Do PT, Caratzoulas S, Lobo RF, Dauenhauer PJ, Vlachos DG (2013) J Catal 297:35–43
18. Nikbin N, Feng S, Caratzoulas S, Vlachos DG (2014) J Phys Chem C 118:24415–24424
19. Rohling RY, Tranca IC, Hensen EJ, Pidko EA (2018) J Phys Chem C 122:14733–14743
20. Rohling RY, Tranca IC, Hensen EJ, Pidko EA (2018) ACS Catal 9:376–391
21. Patet RE, Nikbin N, Williams CL, Green SK, Chang CC, Fan W, Vlachos DG (2015) ACS Catal 5:2367–2375
22. Patet RE, Fan W, Vlachos DG, Caratzoulas S (2017) ChemCatChem 9:2523–2535
23. Li YP, Head-Gordon M, Bell AT (2014) J Phys Chem C 118:22090–22095
24. Chang CC, Cho HJ, Yu J, Gorte RJ, Gulbinski J, Dauenhauer P, Fan W (2016) Green Chem 18:1368–1376
25. Kim TW, Kim SY, Kim JC, Kim Y, Ryoo R, Kim CU (2016) Appl Catal B 185:100–109
26. Williams CL, Chang CC, Do P, Nikbin N, Caratzoulas S, Vlachos DG, Dauenhauer PJ (2012) ACS Catal 2:935–939
27. Song S, Wu G, Dai W, Guan N, Li L (2016) J Mol Catal A Chem 420:134–141
28. Feng X, Shen C, Tian C, Tan T (2017) Ind Eng Chem Res 56:5852–5859
29. Diels O, Alder K (1928) Justus Liebigs Ann Chem 460:98–122
30. Diels O, Alder K (1929) Ber Dtsch Chem Ges 62:554–562
31. Diels O, Alder K (1929) Ber Dtsch Chem Ges 62:2087–2090
32. Fukui K (1982) Science 218:747–754
33. Adjieufack AI, Liégeois V, Mbouombouo Ndassa I, Ketcha Mbadcam J, Champagne B (2018) J Phys Chem A 122:7472–7481
34. Domingo LR, Aurell MJ, Perez P, Saez JA (2012) RSC Adv 2:1334–1342
35. Çelebi-Ölçüm N, Ess DH, Aviyente V, Houk KN (2008) J Org Chem 73:7472–7480
36. Pi Z, Li S (2006) J Phys Chem A 110:9225–9230
37. Domingo LR, Asensio A, Arroyo P (2002) J Phys Org Chem 15:660–666
38. Yamabe S, Minato T (2000) J Org Chem 65(6):1830–1841

39. García JI, Martinez-Merino V, Mayoral JA, Salvatella L (1998) J Am Chem Soc 120(10):2415–2420
40. Suárez D, Sordo TL, Sordo JA (1994) J Am Chem Soc 116:763–764
41. Gonzalez J, Houk KN (1992) J Org Chem 57:3031–3037
42. Guner OF, Ottenbrite RM, Shillady DD, Alston PV (1987) J Org Chem 52:391–394
43. Hamlin TA, Bickelhaupt FM, Fernández I (2021) Acc Chem Res 54:1972–1981
44. Salavati-fard T, Caratzoulas S, Doren DJ (2015) J Phys Chem A 119:9834–9843
45. Domingo LR, Sáez JA (2009) Org Biomol Chem 7:3576–3583
46. Domingo LR (2014) RSC Adv 4:32415–32428
47. Domingo LR, Ríos-Gutiérrez M, Pérez P (2020) Molecules 25:2535–2560
48. Yates P, Eaton P (1960) J Am Chem Soc 82:4436–4437
49. Zhao Y, Truhlar DG (2008) Theor Chem Acc 120:215–241
50. Zhao Y, Truhlar DG (2006) J Chem Phys 125:194101
51. Zhao Y, Truhlar DG (2006) J Phys Chem A 110:13126–13130
52. Lee C, Yang W, Parr RG (1988) Phys Rev B 37:785–789
53. Becke AD (1993) J Chem Phys 98:5648–5652
54. Chai JD, Head-Gordon M (2008) Phys Chem Chem Phys 10(44):6615–6620
55. Dunning TH, Peterson KA, Woon DE (1998). In: Schleyer PVR, Allinger NL, Clark T, Gasteiger J, Kollman P, Schaefer HF III, Schreiner PR (eds) The Encyclopedia Of Computational Chemistry, 1st edn. Wiley, Chichester, p 88
56. Tomasi J, Mennucci B, Cammi R (2005) Chem Rev 105:2999–3094
57. Kelly CP, Cramer CJ, Truhlar DG (2005) J Chem Theory Comput 1:1133–1152
58. Reed AE, Curtiss LA, Weinhold F (1988) Chem Rev 88:899–926
59. Parr RG, Yang W (1989) Density functional theory of atoms and molecules. Oxford University Press, New York
60. Geerlings P, De Proft F, Langenaeker W (2003) Chem Rev 103:1793–1873
61. Domingo LR, Rios-Gutiérrez M, Pérez P (2016) Molecules 21:748–769
62. Parr RG, von Szentpaly L, Liu S (1999) J Am Chem Soc 121:1922–1924
63. Parr RG, Pearson RG (1983) J Am Chem Soc 105:7512–7516
64. Domingo LR, Chamorro E, Pérez P (2008) J Org Chem 73:4615–4624
65. Domingo LR, Aurell MJ, Pérez P, Contreras R (2002) Tetrahedron 58:4417–4423
66. Frisch MJ, Trucks GW, Schlegel HB, Scuseria GE, Robb MA, Cheeseman JR, Scalmani G, Barone V, Mennucci B, Petersson GA, Nakatsuji H, Caricato M, Li X, Hratchian HP, Izmaylov AF, Bloino J, Zheng G, Sonnenberg JL, Hada M, Ehara M, Toyota K, Fukuda R, Hasegawa J, Ishida M, Nakajima T, Honda Y, Kitao O, Nakai H, Vreven T, Montgomery JA, Peralta JE, Ogliaro F, Bearpark M, Heyd JJ, Brothers E, Kudin KN, Staroverov VN, Keith T, Kobayashi R, Normand J, Raghavachari K, Rendell A, Burant JC, Iyengar SS, Tomasi J, Cossi M, Rega N, Millam JM, Klene M, Knox JE, Cross JB, Bakken V, Adamo C, Jaramillo J, Gomperts R, Stratmann RE, Yazyev O, Austin AJ, Cammi R, Pomelli C, Ochterski JW, Martin RL, Morokuma K, Zakrzewski VG, Voth GA, Salvador P, Dannenberg JJ, Dapprich S, Daniels AD, Farkas O, Foresman JB, Ortiz JV, Cioslowski J, Fox DJ (2015) Gaussian 09 Revision E.01. Gaussian Inc, Wallingford CT
67. Jaramillo P, Domingo LR, Chamorro E, Pérez P (2008) J Molec Struct (THEOCHEM) 865:68–72
68. Champagne B, Mosley DH, Fripiat JG, André JM, Bernard A, Bettonville S, François P, Momtaz A (1998) J Molec Struct (THEOCHEM) 454:149–159
69. Champagne B, Cavillot V, André JM, François P, Momtaz A (2006) Int J Quantum Chem 106:588–598
70. Domingo LR, Ríos-Gutiérrez M, Pérez P (2020) RSC Adv 10:15394–15405
71. Domingo LR, Kula K, Ríos-Gutiérrez M (2020) Eur J Org Chem 2020:5938–5948